This is a repository copy of *Investigation on contribution of inductance harmonics to torque production in multiphase doubly salient synchronous reluctance machines*.

# Investigation on Contribution of Inductance Harmonics to Torque Production in Multiphase Doubly Salient Synchronous Reluctance Machines

K. Zhang, G. J. Li, Senior Member, IEEE, Z. Q. Zhu, Fellow, IEEE, and G. W. Jewell

**Abstract—This paper investigates the contribution of each order inductance harmonic to the torque (both average torque and torque ripple) of multiphase doubly salient synchronous reluctance machines (DS-SRMs). Such machines are similar to switched reluctance machines but supplied with sinewave currents. The investigations in this paper are as follows: first, a general analytical torque model based on Fourier Series analysis of inductances has been built for machines with different phase numbers, slot/pole number combinations and also winding configurations. The instantaneous torque for DS-SRMs with any given phase number can then be accurately predicted. Using such model, contribution of each order inductance harmonic to torque can be investigated separately. It is found that the torque ripple frequency of the DS-SRM only depends on phase number. For example, for a m-phase machine, there will be m×k$^{th}$ order torque ripple if $mod(mk, 2) = 0$, where m is phase number and k is a natural number. This study also explains why certain phase numbers inherently produce lower torque ripple than others. The findings in this paper provide a future direction for potential torque ripple reduction methods either from machine design or advanced control. The simulations have been validated by experiments using a 6-phase DS-SRMs.**

**Index Terms—Doubly-salient, multiphase machine, synchronous reluctance machine, torque harmonic.**

## I. INTRODUCTION

SWITCHED reluctance machines (SRMs) have excellent features such as simple and robust structure, high manufacturability, good fault tolerant capability and also low cost. In addition, without permanent magnets or field windings on the rotor, they are particularly suitable for harsh environment operations such as high speed and high temperature. Due to these significant advantages, SRMs have attracted increasing interest in electric vehicles, aerospace and other safety-critical applications [1]-[2]. However, the doubly salient structure together with the special rectangular wave current supply cause high torque ripple, high vibrations and acoustic noise compared with other types of machines. Therefore, in last decades, the torque ripple reduction is one of the most popular research topics for SRMs. This can be achieved from two aspects: machine design [3]-[5] and also advanced control [6]-[7].

One effective and simple way to reduce the torque ripple is to increase the phase number. This method can be applicable not only to SRMs but also to synchronous (reluctance) machines and induction machines. Multiphase machines provide additional benefits apart from the torque ripple reduction

because the machines with higher phase numbers (m>3) can also have higher torque density and better fault-tolerant capability compared with conventional 3-phase machines [8]. Additionally, different winding configurations for multi-phase machines can be selected to achieve even better torque performance [9]-[10].

The conventional SRMs, with 3-phase or multiphase, are supplied with rectangular wave current. However, recent studies have shown that they can be supplied with sinewave currents as well [11]-[12]. It has been found that the sinewave excitations can bring benefit to the radial force reduction for SRMs, which is the primary source of vibrations and acoustic noise. One of the other advantages of sinewave excitation is that the standard 3-phase voltage source inverter as that used in synchronous (reluctance) machines or induction machines can be employed, which can help reduce the system cost. It also provides a more flexible control strategy for SRMs to improve the torque performance. However, it is worth noting that the SRMs with sinewave current supply are actually doubly salient synchronous reluctance machines (DS-SRMs) [13]-[15].

Although the sinewave current supply has the above advantages, it also brings some undesirable side effect, i.e. high torque ripple due to the nature of machine self- and mutual inductances. To analyze the torque ripple mechanisms of different DS-SRMs, finite-element analysis (FEA) are often regarded as effective tools. However, they are more time consuming and cannot really predict the contributions of each inductance harmonic to on-load torque. Other common analytical methods such as Maxwell stress tensor [16]-[17], Virtual work [18]-[19] and Lorentz force law [20]-[21] could be employed. However, due to the doubly salient structure, these methods become extremely complex and hard to implement.

To reduce the modeling complexity, simple analytical torque model based on self- and mutual-inductances has been proposed for the investigated multi-phase DS-SRMs. Although the inductances can be calculated according to winding function theories [18, 22], for simplicity they are calculated by 2D-FEA in this paper. The proposed model can be applied for all kinds of DS-SRMs with different slot/pole combinations and wining configurations, e.g. double-layer (DL), single-layer (SL) and fully-pitched (FP). Through harmonic analysis, the torque ripple frequency and magnitude for DS-SRMs with different phase numbers can be reliably predicted. In addition, the torque contribution due to each inductance harmonic can also be accurately quantified. As a result, the mechanism about why certain phase numbers can have inherently lower torque

Corresponding author: G. J. Li (e-mail: g.li@sheffield.ac.uk).

ripple while others cannot, can be investigated. This will be helpful for researchers to find optimal measures in order to reduce torque ripple of DS-SRMs either from machine design or machine control perspectives.

## II. SRM ANALYTICAL TORQUE MODEL

This paper cover DS-SRMs with various slot/pole combinations and different phase number, e.g., 4s/4p 2-phase, 6s/4p 3-phase, 8s/6p 4-phase, 10s/8p 5-phase, 12s/8p 6-phase and 12/10p 6-phase. By way of example, Fig. 1 shows the cross section and prototype stator and rotor for a double layer 12s/8p 6-phase DS-SRMs. The main specifications for all the topologies are listed in TABLE I. It is worth noting that single layer winding machines have the same key dimensions and also the same number of turns per phase as their double layer counterparts. However, the number of turns per coil of single layer machines will be doubled with the number of coils per phase being halved. In order to achieve optimal performance for multi-phase DS-SRMs, the winding configurations have been designed according to classic winding theory for synchronous machines (fractional slot and also integer slot) [23]-[24].
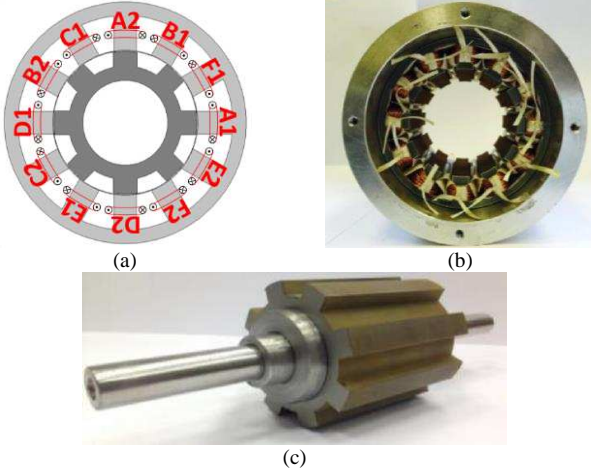


(a)        (b)

(c)

Fig. 1.(a) Cross section, (b) prototype 12-slot stator and (c) 8-poles rotor for a double layer 12s/8p 6-phase DS-SRM.

TABLE I MACHINE KEY DIMENSIONS AND DESIGN FEATURES

| | |
|---|---|
| Stator outer radius (mm) | 45 |
| Split ratio | 0.6 |
| Air gap length (mm) | 0.5 |
| Active length (mm) | 60 |
| Number of turns per phase | 132 |
| Slot fill factor | 0.37 |
| Rated RMS current (A) | 5 |

According to literature, the instantaneous torque equation of SRMs can be obtained based on the phase inductances (self and mutual) and phase currents [2] [3] [25]. Assuming the magnetic saturation can be neglected, the on-load torque of an m-phase SRM is given by

$$T_e = \frac{1}{2}[i_m]^T \frac{d[L_m]}{d\theta}[i_m] \qquad (1)$$

where m represents the phase number, $[i_m] = [i_1, i_2, \cdots i_m]^T$. $[L_m]$ is a $m \times m$ inductance matrix. This equation can also be applicable for DS-SRMs and will be used to investigate the

torque performance in this paper. The general current equation for phase $x$ is written as

$$i_x = I_p \sin\left(\theta_e + \beta - \frac{2\pi}{m}(x-1)\right) \text{ with } x = 1, 2, \cdots m \qquad (2)$$

where $I_p$ is the amplitude of phase current, $\theta_e$ is the electric rotor position, $\beta$ is the current phase angle.

It is worth noting that for a m-phase DS-SRMs, the phase self-inductances have the same magnitude but have a $\frac{2\pi}{m}$ phase shift between them. However, the number of mutual-inductances between phases is a function of phase number $m$, which can be calculated by $m \times (m-1)$. By way of example, Fig. 2 (a) and (b) show the relative phase order in space for 5- and 6-phase machines, respectively. The mutual-inductances between two phases with the same distance in space will have the same waveform but with a $\frac{2\pi}{m}$ phase shift between them. The distance 1 means two phases is adjacent to each other, such as $M_{ab}, M_{bc}, \ldots$; the distance 2 means two phases are not adjacent and have an interval of one phase between them, such as $M_{ac}, M_{bd}, \ldots$Similarly, the distance 3 has an interval of two phases as shown in Fig. 2 (b), such as $M_{ad}, M_{be}, \ldots$ To be more generic, 'Z' can be employed to express the number of different distances between phases for an m-phase DS-SRMs. It is the minimum integer not less than $\frac{C_m^2}{m}$, as shown in (3)
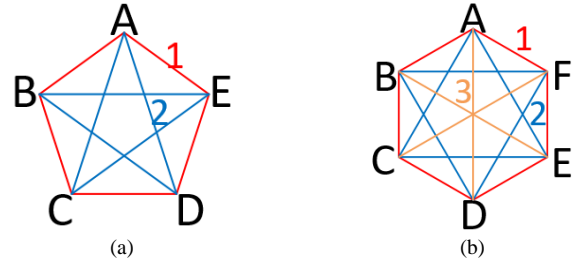


(a)        (b)

Fig. 2. Relative phase order in space for (a) 5-phase and (b) 6-phase DS-SRMs.

$$Z \geq \frac{C_m^2}{m} = \frac{m!}{2!(m-2)! \times m} = \frac{m-1}{2} \qquad (3)$$

By way of example, for the 12s/8p double layer 6-phase DS-SRM, there are 3 types of mutual-inductances due to $\frac{C_6^2}{6} = 2.5$. The inductance waveforms and their spectra are shown in Fig. 3.
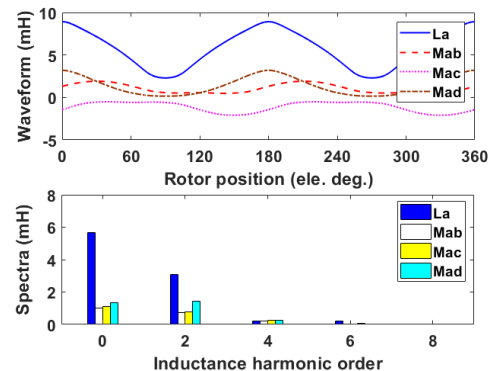


Fig. 3. Inductance waveforms and Spectra of a double layer 6-phase DS-SRM. Calculated by FEA when phase A is supplied with a 1A dc current.

In order to identify the contribution of inductance harmonics to the average torque and torque ripple, the self- and mutual-inductances are expressed using Fourier Series analysis as shown in (4) and (5):

$$L = L_0 + \sum_{n=1}^{\infty} L_n \cos(n\theta_e + \alpha_n) \tag{4}$$

$$M_a = M_{a0} + \sum_{n=1}^{\infty} M_{an} \cos(n\theta_e + \alpha'_{an}) \tag{5}$$

where L and $M_a$ represent the self- and mutual-inductances. $\alpha_n$ and $\alpha'_{an}$ are the phase angles of the $n^{th}$ self- and mutual-inductances, respectively. The subscript '0' represents the dc component of inductances. 'a' represents the distance between two phases and $a \in (1, 2 \cdots Z)$. For example, $M_{10}$ is the dc component of mutual-inductance with the distance 1 in Fig. 2. Substituting (2), (4) and (5) into (1) gives

$$T_e = T_{sel} + T_{mut} \tag{6}$$

with

$$T_{sel} = \frac{mp}{2} \sum_{k=0}^{\infty} \left\{ -\frac{mk}{2} L_{mk} I_p^2 \sin(mk\theta_e + \alpha_{mk}) \right.$$

$$+ \frac{mk-2}{4} I_p^2 L_{mk-2} \sin(mk\theta_e + 2\beta + \alpha_{mk-2}) \tag{7}$$

$$\left. + \frac{mk+2}{4} I_p^2 L_{mk+2} \sin(mk\theta_e - 2\beta + \alpha_{mk+2}) \right\}$$

and

$$T_{mut} = \frac{mp}{2} \sum_{k=0}^{\infty} \sum_{a=1}^{Z} c \left\{ -\frac{mk}{2} I_p^2 M_{amk} \sin(mk\theta_e + \alpha'_{amk}) \right.$$

$$+ \frac{mk-2}{2} I_p^2 M_{a(mk-2)} \sin\left(mk\theta_e + 2\beta + \alpha'_{a(mk-2)} - \frac{2\pi}{m}a\right)$$

$$\left. + \frac{mk+2}{2} I_p^2 M_{a(mk+2)} \sin\left(mk\theta_e - 2\beta + \alpha'_{a(mk+2)} + \frac{2\pi}{m}a\right) \right\} \tag{8}$$

with

$$c = \begin{cases} 0.5 & \mod(m,2) = 0 \text{ and } a = Z \\ 1 & \text{otherwise} \end{cases} \tag{9}$$

where $T_{sel}$ and $T_{mut}$ are the torques produced by the self- and mutual-inductances, respectively. p is the pole-pair number, and k is a natural number. It can be seen that the average torque can be obtained when k is equal to '0'. Moreover, only the interaction between fundamental current and $2^{nd}$ order harmonic inductance can produce the average torque, which can be rewritten as

$$T_0 = \frac{mp}{4} I_1^2 L_2 \sin(-2\beta + \alpha_2)$$

$$+ \frac{mp}{2} \sum_{a=1}^{Z} c I_1^2 M_{a2} \sin\left(-2\beta + \alpha'_{a2} + \frac{2\pi}{m}a\right) \tag{10}$$

According to (6)-(8), it can be proven that for m-phase DS-SRMs, in general, there will be $mk^{th}$ order torque

harmonics when sinewave current is supplied. This is due to the interaction between the fundamental current and the $mk^{th}$, $(mk \pm 2)^{th}$ order inductance harmonics. The contributions of each order inductance harmonic to the torque ripple harmonic are listed in TABLE II. It is worth noting that from the above conclusion, the 3-phase machine will in theory produce triplen order torque harmonics. However, due to the fact that the odd order inductances are equal to zero, therefore the odd order torque harmonics, such as $3^{rd}$, $9^{th}$, $15^{th}$ etc., do not exist. This is the same for the 5-phase machine, in which the $5^{th}$, $15^{th}$, $25^{th}$… order torque harmonics do not exist. Moreover, it can be predicted that the 2-phase and 4-phase machines present the worst performance in terms of torque ripple when sinewave current is supplied. The reason is that all orders of inductance harmonics will contribute to the torque ripple for both types of machine. Even the $2^{nd}$ order inductance (with the highest magnitude, and normally contributes to average torque) will produce the $2^{nd}$ and $4^{th}$ order torque harmonics for the 2-phase machine while produce the $4^{th}$ order torque harmonic for the 4-phase machine. This can explain why certain phase numbers generate higher torque ripple while others do not.

TABLE II ACTIVE INDUCTANCE HARMONICS FOR CERTAIN ORDER TORQUE HARMONICS

| k / m | | 1 | 2 | 3 |
|---|---|---|---|---|
| 2 | Torque | mk=$2^{nd}$ | mk=$4^{th}$ | mk=$6^{th}$ |
| | Inductance | $2^{nd}$, $4^{th}$ | $2^{nd}$, $4^{th}$, $6^{th}$ | $4^{th}$, $6^{th}$, $8^{th}$ |
| 3 | Torque | mk=$3^{rd}$ | mk=$6^{th}$ | mk=$9^{th}$ |
| | Inductance | $1^{st}$, $3^{rd}$, $5^{th}$ | $4^{th}$, $6^{th}$, $8^{th}$ | $7^{th}$, $9^{th}$, $11^{th}$ |
| 4 | Torque | mk=$4^{th}$ | mk=$8^{th}$ | mk=$12^{th}$ |
| | Inductance | $2^{nd}$, $4^{th}$, $6^{th}$ | $6^{th}$, $8^{th}$, $10^{th}$ | $10^{th}$, $12^{th}$, $14^{th}$ |
| 5 | Torque | mk=$5^{th}$ | mk=$10^{th}$ | mk=$15^{th}$ |
| | Inductance | $3^{rd}$, $5^{th}$, $7^{th}$ | $8^{th}$, $10^{th}$, $12^{th}$ | $13^{th}$, $15^{th}$, $17^{th}$ |
| 6 | Torque | mk=$6^{th}$ | mk=$12^{th}$ | mk=$18^{th}$ |
| | Inductance | $4^{th}$, $6^{th}$, $8^{th}$ | $10^{th}$, $12^{th}$, $14^{th}$ | $16^{th}$, $18^{th}$, $20^{th}$ |
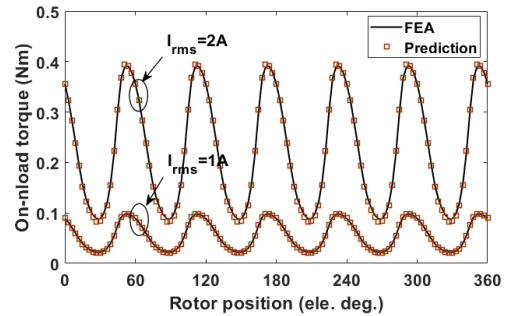


Fig. 4. Comparison of on-load torques between 2D-FEA and analytical prediction for a double layer 12s/8p 6-phase DS-SRM at $I_{rms}$= 1A and 2A.

Fig. 4 shows the comparison results between 2D-FEA and analytical prediction for a double layer 12s/8p 6-phase DS-SRM at 1A and 2A phase RMS current. A generally good agreement can be observed, which validates the accuracy of the proposed analytical torque model. Therefore, only the prediction results of instantaneous torques and spectra are presented for other topologies, as shown in Fig. 5 and Fig. 6, respectively. As expected, the on-load torque of m-phase machines will contain the $mk^{th}$ torque order harmonic if $\mod(mk, 2) = 0$ is valid. However, it is worth noting that for the 12s/10p double layer 6-phase machine, the $6^{th}$ (k=1) order torque ripple can be ignored, which is different from other types

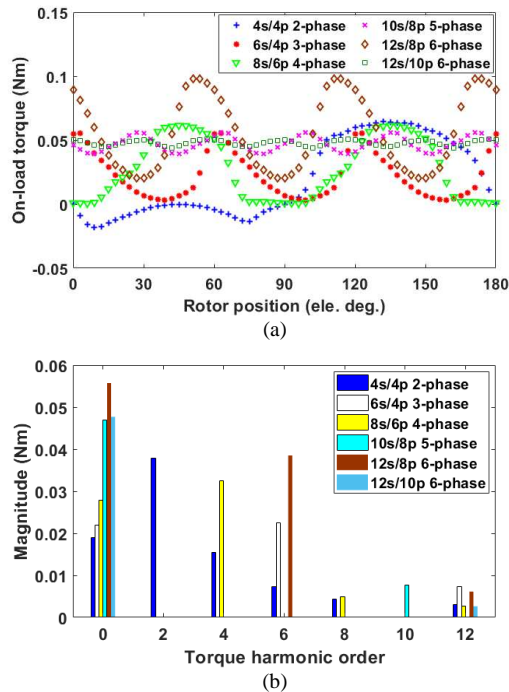of 6-phase machine. This will be investigated further in Section III.



Fig. 5. Predicted results (a) Instantaneous torque and (b) Torque spectra for m-phase double layer DS-SRMs. The machine is supplied with 1A rms current.
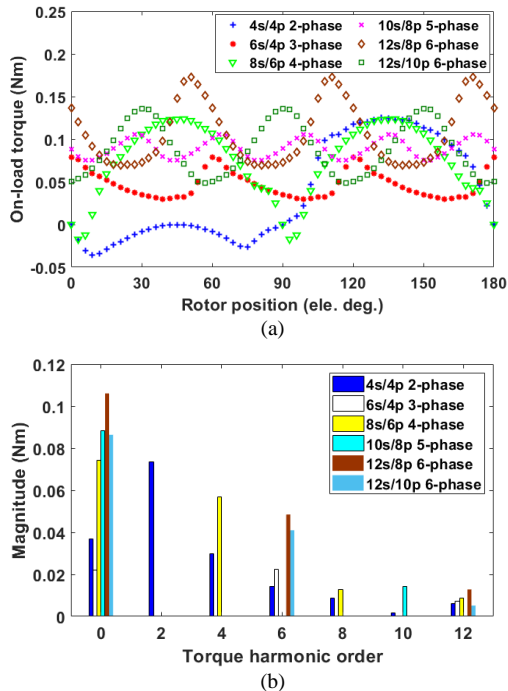


Fig. 6. Predicted results (a) Instantaneous torque and (b) Torque spectra for m-phase single layer DS-SRMs. The machine is supplied with 1A rms current.

## III.   COMPARISON STUDY OF SIX-PHASE TOPOLOGIES

This section will further investigate the influence of machine topologies and winding configurations on torque ripple of the 6-phase machines. Several 6-phase machines (12s/4p, 12s/8p and 12s/10p) with different winding configurations (concentrated and distributed winding) have been considered.

A. Short Pitched Concentrated Winding

By way of example, the two single layer 12s/8p and 12s/10p 6-phase DS-SRMs have been shown in Fig. 7.
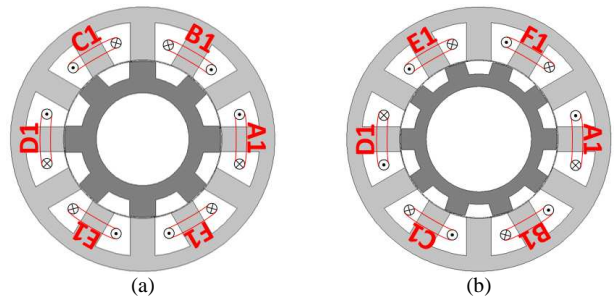


Fig. 7. Two types of 6-phase single layer DS-SRMs. (a) 12s/8p and (b) 12s/10p.
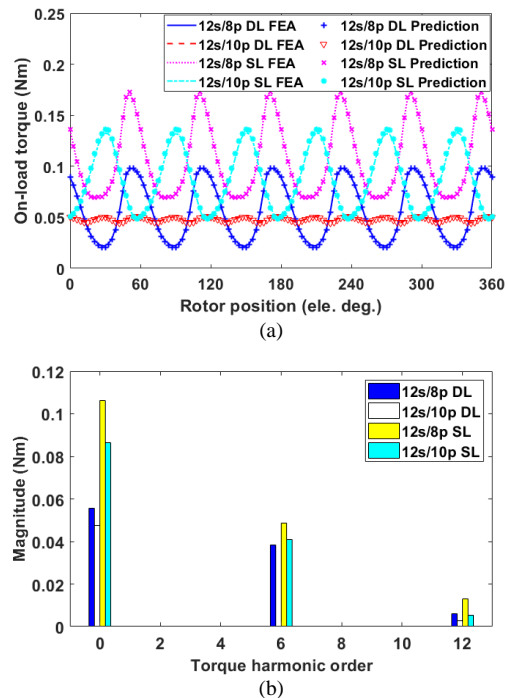


Fig. 8. Comparison of (a) On-load torque and (b) Spectra for 6-phase DS-SRMs. The machines are all supplied with 1A rms current.

According to (6)-(8), the comparison in terms of instantaneous torque and torque spectra for the four types of machines are given in Fig. 8. For different slot/pole number combinations of 6-phase machines, the $6^{th}$, $12^{th}$, $18^{th}$… order torque harmonics will always exist. However, it is obvious from Fig. 8 that the $6^{th}$ order torque harmonic for the 12s/10p double layer machine can be neglected, which is different from other 6-phase machines. In order to figure out the reason behind, the 12s/8p and 12s/10p double layer machines have been further studied. The inductance spectra are shown in Fig. 9. It can be seen that for the two topologies, their inductance harmonic magnitudes have little difference, but the phase angles are significantly different. This will dramatically influence the torque contribution of each inductance harmonic. The torque produced by each inductance harmonic can be predicted by using the proposed torque models (6)-(8), and the results are shown in Fig. 10 and Fig. 11.
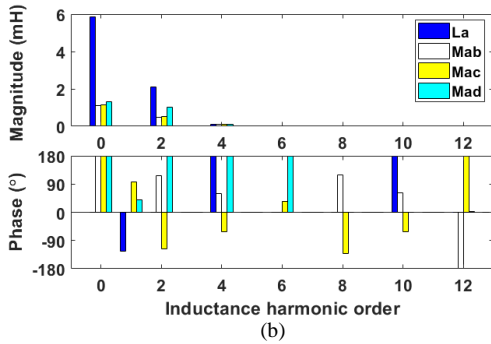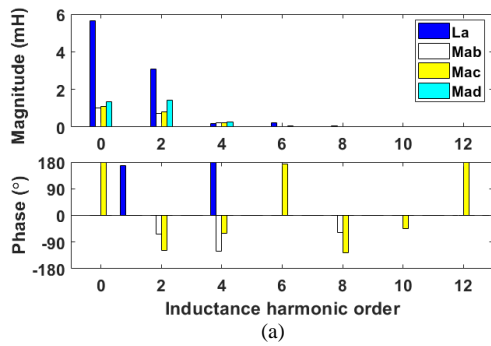
Fig. 9. Magnitudes and phases of inductance harmonics for (a) 12s/8p double layer and (b) 12s/10p double layer DS-SRMs.



Fig. 10. 6th order torque harmonics of the 12s/8p double layer DS-SRMs. (a) Resultant torque, (b) Self- and mutual-torques due to each inductance harmonic. The phase RMS current is 1A.
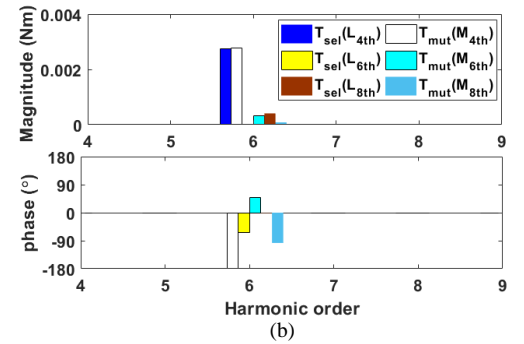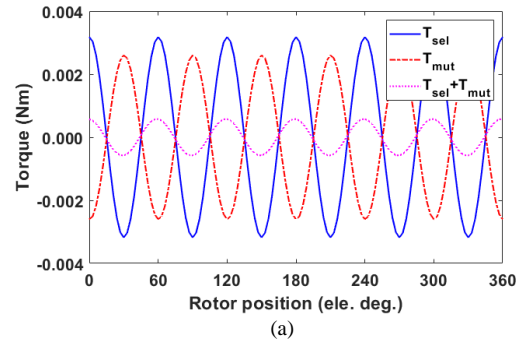


Fig. 11. 6th order torque harmonics of the 12s/10p double layer DS-SRMs. (a) Resultant torque, (b) Self- and mutual-torques due to each inductance harmonic. The phase RMS current is 1A.
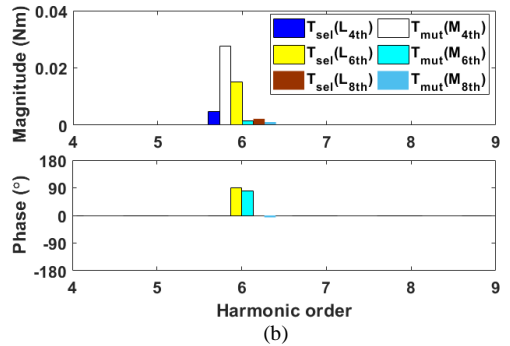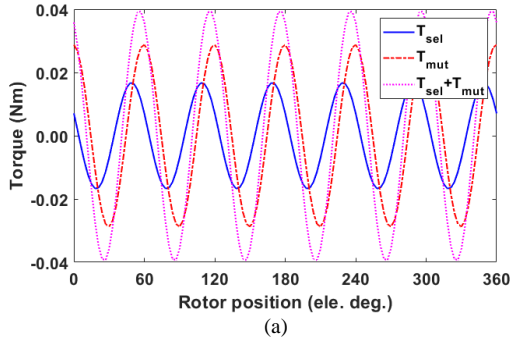
From Fig. 10 and Fig. 11, it can be observed that the 12s/8p machine has much higher magnitudes in torque harmonics for every inductance harmonic than that of the 12s/10p. Moreover, for the 12s/8p machine, the self- and mutual-torques produced by the inductance harmonics have similar phase angles. As a result, the 6th order torque harmonics due to the self- and mutual-inductances are additive, leading to higher overall torque ripple level. In contrast, the self- and mutual-torques of the 12s/10p machine have almost 180 elec. deg. phase difference. This is particularly the case for the self- and mutual-torques due to the 4th order inductance harmonics. As a result, the 6th order torque harmonics for the double layer 6-phase 12s/10p DS-SRMs cancel one another, leading to much lower overall torque ripple level.

It is worth noting that the proposed torque model is based on the phase inductances calculated at low electric loading. With the increasing phase current, the machines become saturated and there is an increasing discrepancy between the results obtained by FEA and the analytical torque models. The average torque and torque ripple coefficient [$(T_{max} - T_{min})/(2T_{ave}) \times 100\%$, where $T_{max}$, $T_{min}$ and $T_{ave}$ are the maximum, minimum and average torques for one electrical period] versus phase root-mean-square (RMS) current, are shown in Fig. 12. It shows that the torque ripple benefit of the 12s/10p machine is not compromised at high saturation level compared with the 12s/8p machine.
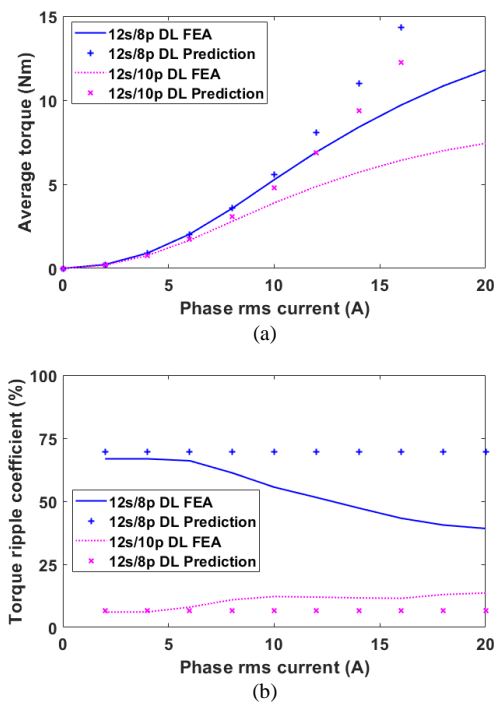
Fig. 12. Comparison of torque production for two topologies. (a) Average torque, (b) Torque ripple coefficient.

B. Fully Pitched Distributed Winding

For completeness, apart from the concentrated winding configurations, 6-phase fully-pitched DS-SRMs with distributed windings have also been investigated in this paper. Their cross-sections and winding configurations are shown in Fig. 13. It is worth noting that the single layer 12s/4p fully-pitched DS-SRMs have exactly the same torque performance as its double layer counterpart. However, the double layer winding does not work for the 12s/8p fully-pitched machines due to negligible torque capabilities. This is because the coil magneto-motive forces of each two opposite phases, e.g. phases A and D, have exactly the same polarity (NN for phase A and NN for phase D as well) at each rotor position, there will be no return path for the armature flux. As a result, the airgap flux density is almost zero, leading to very low output torque. Therefore, only single layer winding topologies have been selected for investigation in this section.
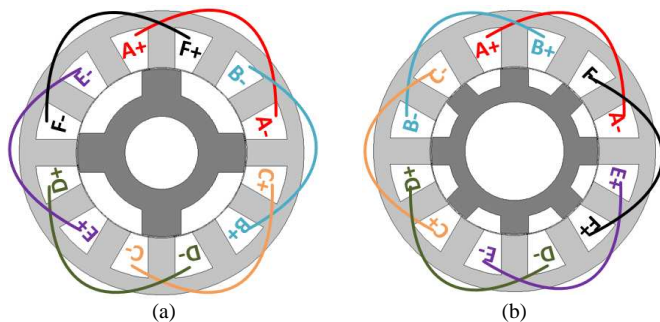


Fig. 13. 6-phase fully-pitched DS-SRMs. (a) 12s/4p, (b) 12s/8p.

The same analyses as in previous sections have been performed for these two machines and the comparison results are shown in Fig. 14. Again, the proposed torque model

provides reliable prediction in terms of on-load torque and there are $6^{th}$, $12^{th}$, $18^{th}$, etc. order torque harmonics as expected.

After comparative studies of different phase numbers, slot/pole number combinations and also winding configurations, one can confirm that for any m-phase DS-SRMs, the torque harmonics due to fundamental current only depend on the phase number 'm' and their orders are equal to mk when $\mathrm{mod}(mk, 2) = 0$. However, without quantifying the contribution of each order inductance harmonic (magnitude) to torque, it is hard to identify which torque harmonic is the most dominant one.
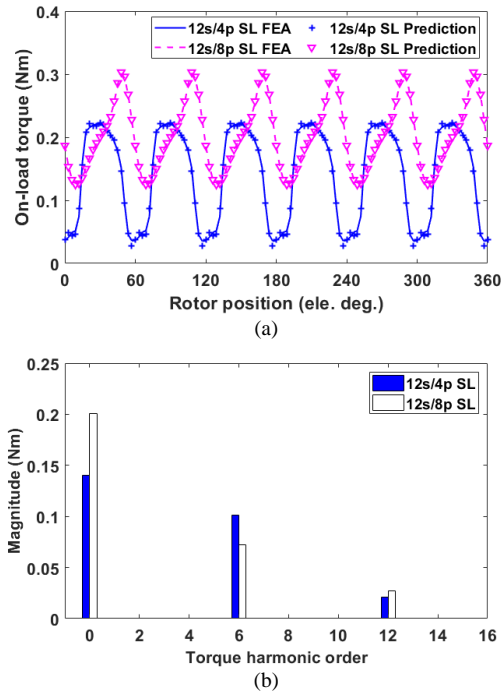


Fig. 14. Comparison of (a) torque and (b) FEA torque spectra for fully-pitched 6-phase DS-SRMs with 1A rms phase current.

## IV. COPPER LOSS FOR MULTIPHASE MACHINE

The investigated machines all have the same number of turns per phase so as to maintain similar phase voltage level. This means that for the same phase current, the copper losses will be different for different phase numbers. To be specific, higher phase number will have higher copper loss ($P_{copper} = mI^2R$, where R is the phase resistance and I is the phase RMS current). In order to achieve fairer comparison, the average torque and torque ripple coefficient versus copper loss have been investigated in this section.

TABLE III PHASE RESISTANCES ACCOUNTING FOR END-WINDINGS FOR DIFFERENT TOPOLOGIES @ 20 ℃

| slot/pole | Phase number | DL (Ω) | SL (Ω) | FP (Ω) |
|-----------|--------------|--------|--------|--------|
| 4s/4p | 2 | 0.638 | 0.789 | - |
| 6s/4p | 3 | 0.766 | 0.893 | - |
| 8s/6p | 4 | 0.993 | 1.111 | - |
| 10s/8p | 5 | 0.985 | 1.089 | - |
| 12s/8p | 6 | 1.02 | 1.116 | 1.617 |
| 12s/10p | 6 | 1.02 | 1.116 | - |
| 12s/4p | 6 | - | - | 1.617 |

The phase resistances for different m-phase machines are listed in TABLE III. Here the different end-winding lengths have been considered, which can be calculated by using the method given in [26].
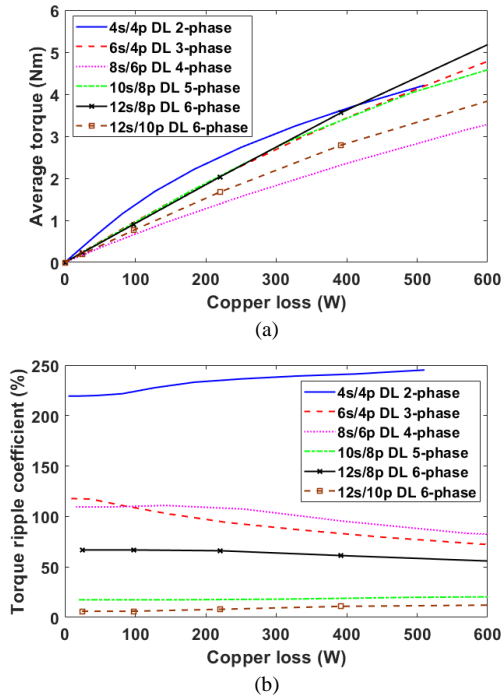


Fig. 15. (a) Average torque and (b) torque ripple coefficient vs copper loss for double layer multiphase machines.
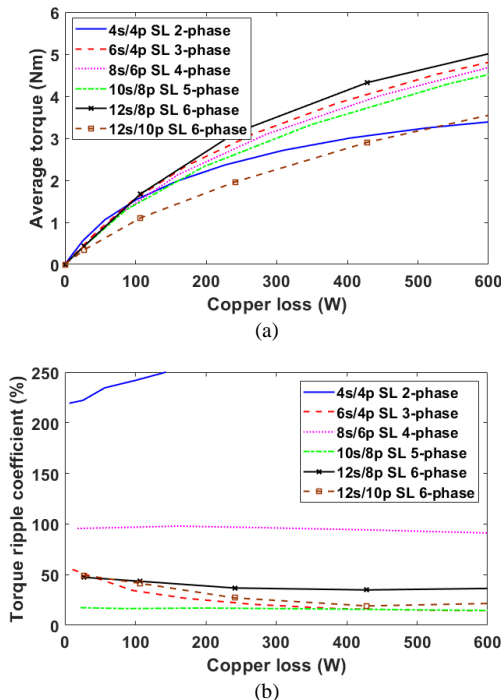


Fig. 16. (a) Average torque and (b) torque ripple coefficient vs copper loss for single layer multiphase machines.

Fig. 15 and Fig. 16 show the average torque and torque ripple coefficient versus copper loss for the double layer and single layer DS-SRMs, respectively. It is found that for both double and single layer winding structures, the 2-phase machines produce higher average torque than other phase numbers at low copper loss. With increasing phase current (or copper loss), the 2-phase machines loss their benefit in terms of average torque, while the 12s/8p 6-phase DS-SRMs will produce the highest average torque at higher copper loss (>400W). 5-phase machines show similar torque capability as the 12s/8p 6-phase machine at lower copper loss, while they have almost the smallest torque ripple coefficient compared with other machines expect the 12s/10p double layer 6-phase machine. In addition, the benefit in terms of torque ripple for the 5-phase machine will not be compromised with increased copper loss. It is also worth noting that the double/single layer 2-phase and 4-phase DS-SRMs have shown much worse torque ripple performance, as expected.
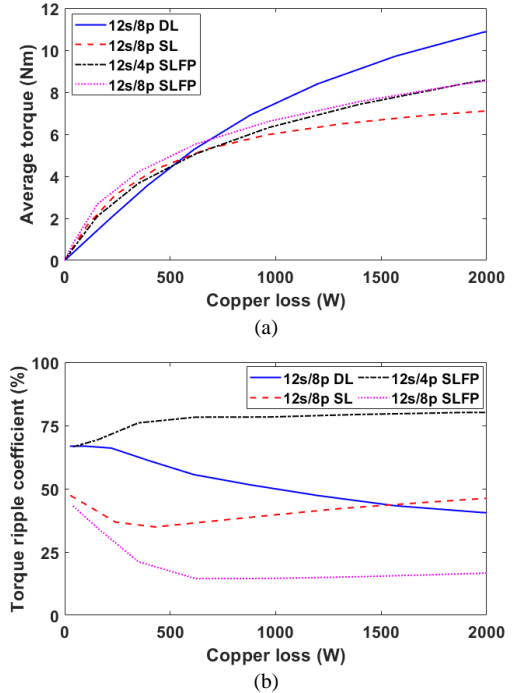


Fig. 17. (a) Average torque and (b) Torque ripple coefficient vs copper loss for 6-phase topologies.

The 12s/8p double/single layer 6-phase machines have also been compared with two types of fully-pitched machines and the results are shown in Fig. 17. It shows when the copper loss is less than 600W, the double layer machines exhibit the lowest average torque compared with other three machines. When the phase current increases, so does the copper loss, the benefit of double layer machines are increasingly evident. It is because they are less sensitive to magnetic saturation due to less flux concentrated in the stator yoke [26]. It is also apparent that the two fully-pitched machines show similar torque capability. However, the 12s/8p fully-pitched machines always achieve the lowest torque ripple compared with other machines, while the 12s/4p fully-pitched machines being the highest. Moreover, it is worth noting that the torque ripple of single layer machines are generally lower than that of double layer machines for lower current (copper loss < 1600W). However, with increasing phase current, this advantage diminishes.

## V. EXPERIMENTAL VALIDATION

### A. Prototypes of SRMs

In order to validate torque capability of proposed 6-phase double layer and single layer DS-SRMs (12s/8p), two prototype DS-SRMs with single layer and double layer windings, which were designed in [26], have been tested as 6-phase models. It is worth noting that all m-phase SRMs in previous section have the same number of turns per phase (132). However, due to the fact that the tested 6-phase machines are converted from 3-phase machines, the number of turns per phase are reduced by half (66). This means that the inductance will be reduced by four times, as shown in Fig. 18. The method of inductance measurement has been introduced in [27]. To be consistent with the prototype machines, the number of turns per phase in the FEA models in the experimental validation section is also reduced to 66.
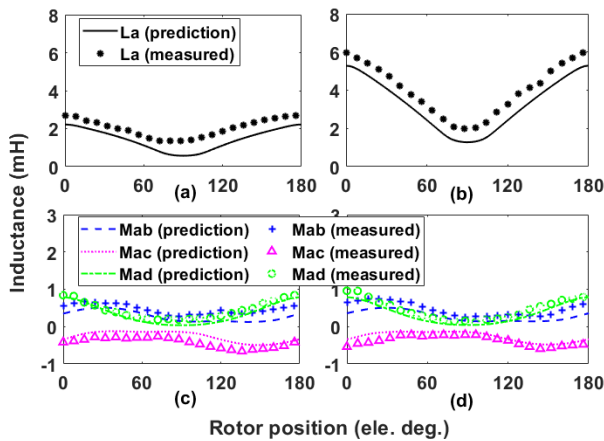


Fig. 18. FEA and measured self-inductance ($L_a$) and mutual inductances with different distance ($M_{ab}$, $M_{ac}$, and $M_{ad}$) for 12s/8p 6-phase DS-SRMs when phase A is supplied with a 2A dc current. (a) and (c) Double layer; (b) and (d) Single layer.

### B. Self- and Mutual-Torque

The method of static torque measurement is detailed in [28] which will be applied to all torque measurement except the on-load static torque in part D. The stator is fixed on the lathe and can be rotated to change the relative angle between rotor and stator, i.e. rotor position, while the rotor shaft is connected with a balance beam and therefore cannot be rotated. There will be pre-load weight at the end of the beam to make sure it has a stable contact with the digital scale. After reading the mass at the end of beam by digital scale, the torque at a fixed rotor position can be calculated by $T_e = (m_r - m_{pre})gl$, where $m_r$ is the mass read from the digital scale, $m_{pre}$ is the mass of pre-load, g is gravitational acceleration and l is the length between the end of the beam and the rotor shaft.

The self-torque can be measured by supplying one single phase with a dc current. For example, 2A dc current is supplied to phase A, and the self-torque $T_a$ can be obtained as shown in Fig. 19. To measure the mutual-torque, firstly, the same level of dc current (2A) is supplied to two phases connected in series, e.g. phases A and B, the resultant torque ($T_a+T_b+T_{ab}$) can be measured for different rotor positions. Then, the mutual torque ($T_{ab}$) can be easily obtained by subtracting self-torques of phases A and B, i.e. $T_a$ and $T_b$, and the results are shown in Fig. 20. It shows that both double and single layer machines have

similar level of mutual-torque. It is worth mentioning that the slight discrepancy between measured and FEA results is probably due to the fact that the end-windings have not been considered in the FEA simulations.
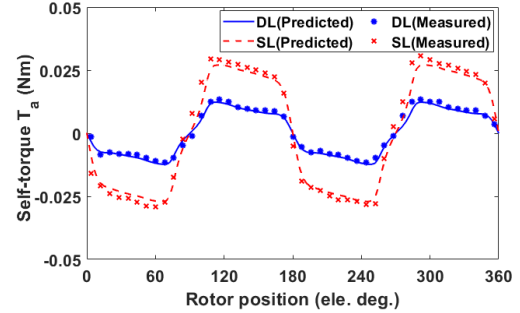


Fig. 19. FEA and measured resultant self-torques $T_a$ for 12s/8p 6-phase DS-SRMs when phase A is supplied with a 2A dc current. (a) Double layer and (b) Single layer.
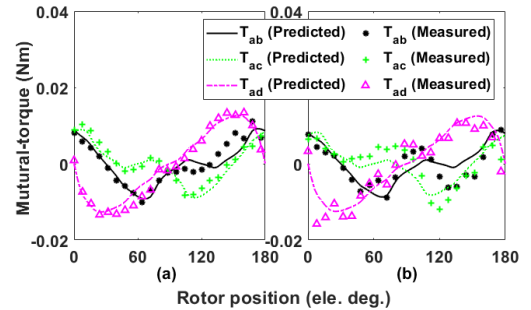


Fig. 20. FEA and measured mutual-torques with different distance for 12s/8p 6-phase DS-SRMs when phase A is supplied with a 2A dc current. (a) Double layer and (b) Single layer.

### C. Static Torque

In this section, machines are tested under a pseudo sinewave current condition ($I_A = I$, $I_B = I/2$, $I_C = -I/2$, $I_D = -I$, $I_E = -I/2$, and $I_F = I/2$), where I is dc current which is 2.83A (2A RMS). The static torque at each rotor position (equivalent to current phase advance angle) can be measured as shown in Fig. 21.

After rotor is locked at the position where the maximum average torque can be achieved (phase advance angle of 45° for synchronous reluctance machines), the static torque against phase RMS current can be measured and compared with FEA results, as shown in Fig. 22. Overall, good agreement can be observed between the predicted and measured results.
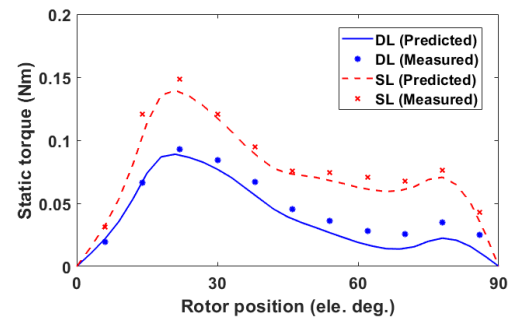


Fig. 21. FEA and measured static torques versus rotor position at 2A phase RMS current for 12s/8p 6-phase DS-SRMs.
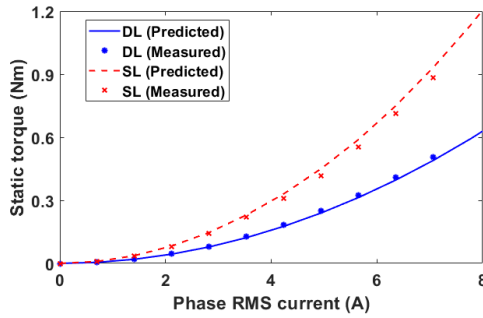
Fig. 22 FEA and measured static torques versus phase RMS current for 12s/8p 6-phase DS-SRMs.

### D. On-load Static Torque

In order to measure on-load static torque vs rotor positions for 6-phase DS-SRMs under sinewave excitation, at least 4 current generators are required if using the same measurement methods as in previous section. This is very inconvenient. However, it is much easier to use two 3-phase half-bridge inverters to control the 6-phase currents. During the test, the rotors are locked at different rotor positions. At each rotor position, 6-phase dc currents are supplied to the machines, and the amplitudes of these currents are chosen according to the values of 6-phase sinewave currents at different rotor positions. The torque can then be measured by torque transducer. It is worth noting that, due to the inaccuracy of the torque transducer, higher phase RMS current (5A) has been chosen in this test in order to improve the signal to noise ratio. Fig. 23 shows the predicted and measured on-load torques.
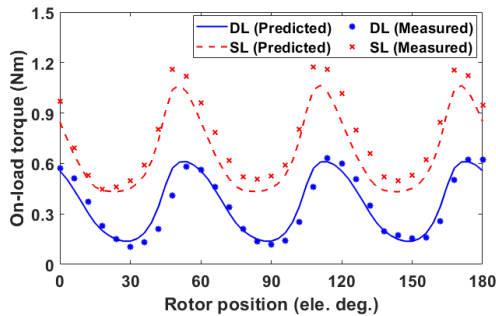


Fig. 23 FEA and measured on-load static torques for 12s/8p 6-phase DS-SRMs versus rotor position at 5A phase RMS current.

## VI. Conclusion

This paper proposes a general instantaneous torque prediction methods for multiphase doubly salient synchronous reluctance machines (DS-SRMs). The torque produced by each inductance harmonic can be accurately predicted. Based on the analytical torque equation, it is found that for the DS-SRMs, the torque harmonic frequency only depends on the phase number. Generally, there will be $mk^{th}$ order torque harmonics for m-phase machine if $\mod(mk, 2) = 0$ is valid, and they are due to the interaction between the fundamental current and the $mk^{th}$, $(mk \pm 2)^{th}$ order inductance harmonics. However, there is also a special case such as the 12s/10p double layer 6-phase machines which have self- and mutual- $6^{th}$ order torque harmonics cancelled one another and inherently lead to much lower torque ripple.

Moreover, it is also found that the 2- and 4-phase machines will produce inherently higher torque ripple due to the fact that all the inductance harmonics contribute to torque ripple. However, for the 5-phase machines, only certain inductance harmonics contribute to torque ripple. Other inductance harmonics, particularly some low order inductance harmonics (n<8), with relative higher magnitudes, have no influence on torque ripple. As a result, the 5-phase machines generally achieve lower torque ripple than other phase numbers. Two prototype 6-phase machines with both single layer and double layer windings have been used for experimental validations.

## References

[1] C. Gan, J. Wu, Q. Sun, W. Kong, H. Li, and Y. Hu, "A review on machine topologies and control techniques for low-noise switched reluctance motors in electric vehicle applications," IEEE Access, vol. 6, pp. 31430-31443, May 2018.

[2] X. Deng, B. Mecrow, H. Wu, and R. Martin, "Design and development of low torque ripple variable-speed drive system with six-phase switched reluctance motors," IEEE Trans. Energy Conver., vol. 33,(1) pp. 420-429, Mar. 2018.

[3] D. H. Lee, T. H. Pham, and J. W. Ahn, "Design and operation characteristics of four-two pole high-speed SRM for torque ripple reduction," IEEE Trans. Ind. Electron., vol. 60,(9) pp. 3637-3643, Sep. 2013.

[4] L. Huang, J. Feng, S. Guo, Y. F. Li, J. Shi, and Z. Q. Zhu, "Rotor shaping method for torque ripple mitigation in variable flux reluctance machines," IEEE Trans. Energy Conver., vol. 33,(3) pp. 1579-1589, Sep. 2018.

[5] G. J. Li, X. Ma, G. Jewell, and Z. Q. Zhu, "Novel modular switched reluctance machines for performance improvement," IEEE Trans. Energy Conver., vol. 33,(3) pp. 1255-1265, Sep. 2018.

[6] Q. Ze, D. Liang, P. Kou, and Z. Liang, "Reduction of torque and voltage ripple in a doubly salient permanent magnet generator," IEEE Trans. Energy Conver., vol. 33,(2) pp. 702-715, Jun. 2018.

[7] C. Lai, G. Feng, K. Mukherjee, V. Loukanov, and N. C. Kar, "Torque ripple modeling and minimization for interior PMSM considering magnetic saturation," IEEE Trans. Power Electron., vol. 33,(3) pp. 2417-2429, Mar. 2018.

[8] L. Parsa, "On advantages of multi-phase machines," 31st Annual Conf. IEEE Ind. Electron. Society (IECON 05), p. 6, 6-10 Nov. 2005.

[9] X. Deng, B. Mecrow, R. Martin, and S. Gadoue, "Effects of winding connection on performance of a six-phase switched reluctance machine," IEEE Trans. Energy Conver., vol. 33,(1) pp. 166-178, Mar. 2018.

[10] G. J. Li, J. Ojeda, E. Hoang, M. Lecrivain, and M. Gabsi, "Comparative studies between classical and mutually coupled switched reluctance motors using thermal-electromagnetic analysis for driving cycles," IEEE Trans. Magn., vol. 47,(4) pp. 839-847, Apr. 2011.

[11] X. Liu, Z. Q. Zhu, M. Hasegawa, A. Pride, and R. Deodhar, "Investigation of PWMs on vibration and noise in SRM with sinusoidal bipolar excitation," in Proc. 21th IEEE International Symposium on Ind. Electron., Hangzhou, China, pp. 674-679, May 28-31 2012.

[12] X. B. Liang, G. J. Li, J. Ojeda, M. Gabsi, and Z. X. Ren, "Comparative study of classical and mutually coupled switched reluctance motors using multiphysics finite-element modeling," IEEE Trans. Ind. Electron., vol. 61,(9) pp. 5066-5074, Sep. 2014.

[13] C. M. Spargo, B. C. Mecrow, J. D. Widmer, and C. Morton, "Application of fractional-slot concentrated windings to synchronous reluctance motors," IEEE Trans. Ind. Appl., vol. 51,(2) pp. 1446-1455, Mar.-Apr. 2015.

[14] C. M. Spargo, B. C. Mecrow, J. D. Widmer, C. Morton, and N. J. Baker, "Design and validation of a synchronous reluctance motor with single tooth windings," IEEE Trans. Energy Convers., vol. 30,(2) pp. 795-805, Jun. 2015.

[15] C. M. Donaghy-Spargo, B. C. Mecrow, and J. D. Widmer, "On the influence of increased stator leakage inductance in single-tooth wound synchronous reluctance motors," IEEE Trans. Ind. Electron., vol. 65,(6) pp. 4475-4482, Jun. 2018.

[16] D. Zarko, D. Ban, and T. A. Lipo, "Analytical solution for electromagnetic torque in surface permanent-magnet motors using conformal mapping," IEEE Trans. Mag., vol. 45,(7) pp. 2943-2954, Jul. 2009.

[17] B. Gaussens, O. D. l. Barrière, E. Hoang, J. Saint-Michel, P. Manfe, M. Lécrivain, et al., "Magnetic field solution in doubly slotted airgap of

conventional and alternate field-excited switched-flux topologies," IEEE Trans. Mag., vol. 49,(9) pp. 5083-5096, Sep. 2013.

[18] S. Jia, R. Qu, J. Li, and D. Li, "Principles of stator dc winding excited vernier reluctance machines," IEEE Trans. Energy Conver., vol. 31,(3) pp. 935-946, Sep. 2016.

[19] W. Xinghua, L. Qingfu, W. Shuhong, and L. Qunfeng, "Analytical calculation of air-gap magnetic field distribution and instantaneous characteristics of brushless DC motors," IEEE Trans. Energy Conver., vol. 18,(3) pp. 424-432, Sep. 2003.

[20] L. R. Huang, J. H. Feng, S. Y. Guo, J. X. Shi, W. Q. Chu, and Z. Q. Zhu, "Analysis of torque production in variable flux reluctance machines," IEEE Trans. Energy Conver., vol. 32,(4) pp. 1297-1308, Dec. 2017.

[21] N. Bianchi, S. Bolognani, D. Bon, and M. D. PrÉ, "Torque harmonic compensation in a synchronous reluctance motor," IEEE Trans. Energy Convers., vol. 23,(2) pp. 466-473, Jun. 2008.

[22] T. A. Lopo, Analysis of synchronous machines,. 2nd ed. Boca Raton, USA: CRC Press, 2008.

[23] N. Bianchi and M. D. Pre, "Use of the star of slots in designing fractional-slot single-layer synchronous motors," IEE Proceedings - Elect. Power Appl., vol. 153,(3) pp. 459-466, May 2006.

[24] E. Fornasiero, L. Alberti, N. Bianchi, and S. Bolognani, "Considerations on selecting fractional-slot nonoverlapped coil windings," IEEE Trans. Ind. Appl., vol. 49,(3) pp. 1316-1324, May-Jun. 2013.

[25] Z. Q. Zhu, B. Lee, L. Huang, and W. Chu, "Contribution of current harmonics to average torque and torque ripple in switched reluctance machines," IEEE Trans. Magn., vol. 53,(3) pp. 1-1, Mar. 2017.

[26] X. Y. Ma, G. J. Li, G. W. Jewell, Z. Q. Zhu, and H. L. Zhan, "Performance comparison of doubly salient reluctance machine topologies supplied by sinewave currents," IEEE Trans. Ind. Electron., vol. 63,(7) pp. 4086 - 4096, Jul. 2016.

[27] G.-J. Li, X. Ma, G. Jewell, Z. Q. Zhu, and P. Xu, "Influence of conduction angles on single layer switched reluctance machines," IEEE Trans. Mag., vol. 52,(12) pp. 1-1, Dec. 2016.

[28] Z. Q. Zhu, "A simple method for measuring cogging torque in permanent magnet machines," in Proc. IEEE Power Energy Soc. Gen. Meeting, pp. 1-4, Jul. 2009.